Molecular and Thermodynamic Insights into Interfacial Interactions Between Collagen and Cellulose Investigated by Molecular Dynamics Simulation and Umbrella Sampling

Huaiqin Ma
Shaanxi University of Science & Technology
Qingwen Shi
Shaanxi University of Science & Technology
Xuhua Li
Xi'an Jiaotong University
Junli Ren
Shaanxi University of Science & Technology
Zhijian Li
Shaanxi University of Science & Technology
Lulu Ning (ninglulu@sust.edu.cn)
Shaanxi University of Science & Technology

Research Article

Keywords: cellulose, collagen, molecular dynamics simulation, umbrella sampling

Posted Date: September 21st, 2022

DOI: https://doi.org/10.21203/rs.3.rs-1958275/v2

Abstract

Cellulose/collagen composites have been widely used in biomedicine and tissue engineering. Interfacial interactions are crucial in determining the final properties of cellulose/collagen composite. Molecular dynamics simulations were carried out to gain insights into the interactions between cellulose and collagen. It has been found that the structure of collagen remained intact during adsorption. The results derived from umbrella sampling showed that (110) and (1-10) faces exhibited the strongest affinity with collagen, (100) face came the second and (010) the last, which could be attributed to the surface roughness and hydrogen-bonding linkers involved water molecules. Cellulose planes with flat surfaces and the capability to form hydrogen-bonding linkers produce stronger affinity with collagen. The occupancy of hydrogen bonds formed between cellulose and collagen was low and not significantly contributive to the binding affinity. These findings provided insights into the interactions between cellulose and collagen at the molecular level, which may guide the design and fabrication of cellulose/collagen composites.

1. Introduction

Cellulose is a non-branched natural polymer composed of repeating glucose units ($C_6H_{10}O_5$) [1] and is considered as the most abundant natural polymer in the biosphere. Cellulose naturally has the advantages including low density, low price, as well as biodegradability. Functionality, flexibility, and high specific strength of cellulose have further been developed by exploiting its hierarchical structure that covers from nanoscale to macroscale in various forms including nanocrystalline, aggregates, fbrils and so on [2, 3]. The application of cellulose as renewable and biodegradable raw material in various fields is a proposed solution to the recent industrial challenge to successfully meet environmental and recycling criteria. Traditionally, cellulosic materials have been used in industries for developing paper and textile. While in the last decades, nanostructures obtained by disintegration of cellulose fibers yielding nano- or microfibrillated cellulose and cellulose whiskers laid the foundation for the development of novel materials with extraordinary properties. Nowadays, cellulosic materials have been used for a variety of applications, such as wound treatment [4], tissue engineering [5], drug delivery [6], energy storage systems [7], sensors [8] and biosensors [9].

Collagen is one of the most abundant and widely distributed proteins in the human body [10]. It is the main component of tendons, bone tissue, skin, ligaments, corneas and many interstitial connective tissues [11]. Collagen can also be a candidate for biomaterials such as tissue-engineered scaffolds and wound dressings [10, 12, 13]. However, the application of pure collagen materials is limited due to their low water resistance, fast biodegradation perishability, and poor thermal stability [13], while cellulose/collagen composite materials overcome the weaknesses of pure collagen materials. Researchers [14] have proved that nanocellulose/collagen composite has water resistance, strength and stability better than pure collagen. Animal experimental studies of cellulose/collagen nanofiber hydrogel scaffold showed that the composite scaffold had good porous structure and physical stability and could be used in bone tissue engineering [5]. It also had good biocompatibility and was conducive to cell

adhesion and growth [15], demonstrating that collagen and nanocellulose composite is a promising material for wound dressings and tissue engineering scaffolds. The incorporation of cellulose is a convenient and promising way to reinforce collagen without impairing biocompatibility and biodegradability, which show great promise as cost-effective forward-looking materials for biomedical applications.

As potential biomedical material, the practical application values of cellulose/collagen composites are largely dictated by their physicochemical properties. For example, scaffolds must have sufficient mechanical strength such as tensile strength, yield strength and elastic modulus to maintain their structural integrity in the process of during transport, surgical handling and implantation. Engineered scaffolds should typically mimic the mechanical properties of their target tissue and therefore controllable regulation of mechanical properties is essential when confronting various tissues with distinctive mechanical features such as bone, cartilage scaffolds. Furthermore, density, melting point, and water absorption rate of composite also affect the application of biomaterials. These properties of composites are closely relevant to interfacial interactions [16, 17], which largely determined the macroscopic physical properties of materials. Therefore, the elucidation of collagen and cellulose interactions is crucially important to instruct the design and optimization of composite materials. In addition to interfacial interactions, the effects of cellulose on the structure of collagen also impact the properties of composite materials. Therefore, it is necessary to study the interactions between cellulose and collagen to further improve the performance of the composite material.

The interaction between cellulose and protein complex is very complex, including hydration, cross-linking, covalent and non-covalent bonds between components [18]. The majority of studies investigated the interactions between cellulose and protein and focused on cellulose binding modules (CBMs). Several studies have established that three aromatic residues on a CBM surface were critical for binding onto cellulose crystals and that tryptophans contributed more to binding affinity than tyrosines [19, 20]. CBMs have well-defined binding sites and tend to bind on hydrophobic (110) plane of Iα crystal [21]. The binding forces between different cellulosic nanomaterials and cellulose binding modules family belonging to cellulase have been investigated by single molecule force spectroscopy. It has been found that CBM1 had a similar interaction force on the surfaces of unmodified cellulose regardless of the degree of crystallinity and morphology [22]. Force spectroscopy measurements and molecular dynamics simulations indicated that CBM1 displayed lower binding affinity toward cellulose III [23]. However, only a few studies focused on the interactions between cellulose and collagen. Two-dimensional Fourier transform infrared spectroscopy analysis confirmed the hydrogen bonding and electrostatic interactions between succinylated collagen and carboxymethyl cellulose [24]. Although there have been experimental studies on the interaction between collagen and cellulose, the specific interaction and structural characteristics of collagen in the matrix has not been clearly stated [25]. The molecular-level interaction between cellulose and collagen is still obscure, which may limit the rational development of new cellulose/collagen composites with ideal physical and chemical properties.

Native crystalline cellulose contains a mixture of crystal faces [26], which complicates the direct assignment of cellulose-collagen interactions to a specific face by experimental methods such as NMR spectroscopy. Molecular dynamics simulations (MD) provide a good solution to bypass this limitation and a single crystal face in nanoscale can be constructed by molecular modeling. Molecular dynamics simulations have been carried out by Crowley et al. to study the interactions between cellulose and lignin and gained insights into quantitative relationships between different cellulose faces and specific lignin chemistries [27]. Molecular dynamics simulations have also been used to probe the interactions between water molecules and cellulose, which shed light on the wetting mechanisms of cellulose [28]. Herein, molecular dynamics simulations were carried out in this study to investigate the interactions between collagen and four crystal planes of cellulose.

In this work, Iβ-cellulose, which is one of the main components of higher plants [29], was selected to model cellulose. The adsorption of collagen on different crystal planes of cellulose was simulated by molecular dynamics. Considering the different molecular structures and hydrophilicity of the exposed surfaces of cellulose, non-polar (100), polar (1-10), (110) and (010) with distinct roughness have been studied. The binding energy are evaluated by umbrella sampling and the key factors driving the combination of cellulose and collagen are discussed, which provide molecular insights into the interfacial interactions and gain insights into the possible strategies to improve the performance of cellulose/collagen composites.

2. Methods

The dominant natural crystalline cellulose polymorph exhibits four potential crystalline faces ((100), (110), (1-10) and (010)) with significant surface area (Fig. 1A). The crystalline cellulose faces were built based on an initial cellulose Iβ crystal constructed Cellulose-Builder [30]. The number of repeating units in each face wa

s chosen such that the size of cellulose could accommodate the collagen. The thickness of cellulose sheets ranged from 2.0~4.0 nm in order to keep the core structure stable in the process of simulation. The initial structure of collagen was obtained by extracting three chains from the crystal structure (PDB code 1K6F) [31] as shown in Fig. 1B, which is the most investigated model in structural studies of collagen. Collagen was placed above the surface of the cellulose crystal in different orientation with the angles between collagen main axis and cellulose plane being 0º, 30º and 45º respectively. VMD [32] was used to build all the models and 12 different systems were produced with the minimum distances between collagen and cellulose face ranging from 0.8 nm to 1.0 nm (Fig. 2A). The composite system was solvated in a cubic box with a TIP3P water model [33, 34] and modeled by a CHARMM36 force field [34, 35].

All MD simulations were performed in GROMACS-5.1 package [36, 37]. All the systems were equilibrated carefully in the beginning of simulation. The energy minimization process was carried out with 1000 cycles of steepest descent and 1000 cycles of conjugate gradient minimization. Then, equilibration runs

were performed for 5 ns in the NVT ensemble and 5 ns in the NPT ensemble with protein backbone fixed. Finally, 500 ns production runs were simulated in the NPT ensemble with protein released. The long-range electrostatic interactions were treated by the particle mesh Ewald (PME) method [38], while the short-range van der Waals interactions were calculated with a cutoff distance of 1.0 nm. All covalent bonds containing hydrogen atoms were constrained by the LINCS algorithm [39]. The V-rescale thermostatic [40] was used to heat the system to 300 K and the Parrinello-Rahman Pressure coupling [41, 42] kept the system pressure at 1 bar. The integration step size of the simulation process is 2 fs. Periodic boundary conditions were applied in all directions with covalent glycosidic bonds formed between mirror images.

The potential of mean force [43] (PMF) obtained by pulling simulation and umbrella sampling [44] was used to calculate the binding free energy of the system. The cellulose surface was used as a reference point and a harmonic potential was applied to the collagen as a pulling point. The last frame of the MD simulations was selected as the initial conformation, 300 ps umbrella traction was provided for collagen along the z-axis to increase the center of mass (COM) distance between collagen and cellulose. The spring constant used was 2000 kJ mol^{-1} nm^{-2} and the pull rate was 0.01 nm/ps. More than 13 umbrella sampling windows were selected according to the interval size of COM values. 1 ns pressure equilibrium was performed on each sample, then 10 ns of dynamic simulation process was carried out. Finally, weighted histogram analysis [44] (WHAM) was used to calculate PMF.

The relevant modules in GROMACS were used to calculate the backbone root mean square deviation (RMSD), backbone root mean square fluctuation (RMSF) and radius of gyration (Rg) of proteins during the whole simulation process. When the distance between two atoms is less than 0.5 nm, the two atoms were in contact. The number of hydrogen bonds was calculated with the Donor-Acceptor distance 0.30 nm and Hydrogen-Donor-Acceptor 30° as criterial. VMD was employed to render all the structures.

3. Results And Discussion

3.1 Structural stability of collagen on the four faces of cellulose

The (100) face is hydrophobic and the surface is unable to form significant hydrogen bonds with other molecules due to the orientation of cellulose hydroxyl groups. The (110), (1-10) faces and the (010) face are hydrophilic with abundant hydrogen bond interaction sites [45]. Though the hydrophobicity of each face was distinctive, the collagens were all adsorbed on the surfaces of cellulose. As shown in Fig. 2B-E, the surfaces of cellulose still maintain the significant features of crystal faces with insignificant structural disturbances. No obvious structural changes are observed except that the overall structures of collagen are slightly bent at the end of the simulation.

The RMSD of collagen backbone was calculated to quantitatively measure the change of collagen structure during the simulation. RMSD values of collagen on different cellulose crystal faces are kept between 0.2 nm-0.3 nm as shown in Fig. 3A-D. The profiles of RMSD exhibit very small fluctuation during

the whole process. RMSD values in this range indicate that the protein structures remain stable during the adsorption process. Furthermore, RMSF was calculated to evaluate the free movement degree of each residue in collagen molecules. As shown in Fig. 3E-H, the profiles of RMSF has good accordance with each other regardless of the properties of different cellulose faces. Each chain of the collagen model is composed of 29 residues and the peak of the line represents the end of each chain, which indicates that the two ends of the polypeptide chain are more flexible and the structure of other residues located in the middle of collagen is stable. The overall structures of collagen are not damaged during the process of adsorption on different crystal faces of cellulose.

To analyze the structural changes of collagen in the process of adsorption in more detail, the Ramachandran plot [46] was employed to characterize the changes in the secondary structure of proteins. Collagen is a coil, but one with distinct tertiary and quaternary structures: three separate polypeptides, called α chains are supertwisted about each other. The superhelical twisting is right-handed in collagen, opposite in sense to the left-handed helix of the α chains. Thus, it is ambiguous to evaluate the secondary structure of collagen by designating the structure helix, sheet, or coil. Therefore, Ramachandran plots were employed. The collagen helix is a unique secondary structure with Phi=-51°and Psi =+153°, which is quite distinct from the α helix [47]. As shown in Fig. 4, Ramachandran plots of the last frames extracted from the three MD simulations display similar characteristics and most of Phi and Psi values are confined within the region corresponding to the structure of collagen. It is found by comparison that the Phi and Psi angles of collagen not significantly deviated (Fig. 4A-D) from the specified collagen conformation values during the adsorption of collagen in different crystal faces of cellulose. Therefore, it is indicated that all models exhibit partial structural interruption but are not damaged during adsorption.

To further investigate the effects of cellulose on the global structure of collagen, free energy contour maps were constructed with RMSD and Rg as reaction coordinates. As shown in Fig. 5, the free energy contour values of each model are located in a similar region with only one global minimum, which indicates that the effects of different crystal face on collagen structures are too weak to induce obvious changes. All the global minima of the 12 MD simulations are restricted within narrow ranges with RMSD about 0.23 nm and Rg about 0.42 nm, which further validates the intactness of collagen on the surface of cellulose. The conformational space of collagen on the surface of cellulose provided information about the structural state of collagen in cellulose/collagen composites.

3.2 Interactions between collagen and celluloses during adsorption

To understand the adsorption of collagen onto cellulose, umbrella sampling simulations were performed for all the four faces. Prior to the umbrella sampling simulations, the centers of all the cellulose models move to original points. As shown in Fig. 6, the lowest PMF values are found near the layer surface for all the systems, indicating that collagen tends to bind to cellulose. PMF shows that free energies are close for faces (110) and (1-10) with values of -15.5 kcal/mol and -14.8 kcal/mol respectively, which imply almost the same adsorption strength of collagen onto the (110) and (1-10) surface. Free energy of (100)

(-9.5 kcal/mol) is a little higher than those of (110) and (1-10) faces, indicating that the affinity between (100) layer and collagen is weaker. In contrast with PMF profiles of (110), (1-10), and (100), the binding energy of (010) is the largest (-5.2 kcal/mol). These free energies derived from umbrella samplings indicate that collagen tends to migrate toward all the faces of cellulose. In particular, (110) and (1-10) faces displaying the strongest affinity to collagen.

To characterize the binding process of collagen on cellulose, we calculated the number of collagen heavy atoms that are within 0.5 nm to the four crystal faces over time. As depicted in Fig. 7A, the contact profiles of the three (100) replicas show commendable consistency with no significant changes after 200 ns. Similarly, two stages of contact numbers are also observed (Fig. 7G) when collagen binds to (010) face: an initial stage with contact numbers ranging from 0 to about 180 (0-100 ns) and a stable final stage with contact number fluctuating around 180. As for (110) and (1-10) face, the profile of contact numbers varies but all the collagens form stable binding with cellulose after 250 ns. In general, collagen adsorbed onto cellulose spontaneously and form stable combination with cellulose. Due to the structural anisotropy of cellulose, the four faces exhibit different values of contact numbers in the last stages.

In order to further clarify the molecular mechanism underlying the difference of binding energy, the distributions of contact numbers have been calculated. As shown in Fig. 7B, D, F and H, compared with (100), (110) and (1-10), the (010) face display the minimum contact number with the peaks corresponding to about 180. The profiles of contact numbers belonging to (110) and (1-10) faces are similar but move to the right in contrast with that of (010) face, which indicate more intimate contact with cellulose. (100) face exhibit the largest contact number among the four faces. The origin of this this phenomenon can be attributed to the topography of cellulose crystal faces. The (010) surface is saw-toothed (Fig. 8D), while the (100) surface is almost flat (Fig. 8A), and the (010) surface is expected to have a roughness much higher than the other three surfaces. (110) and (1-10) faces exhibit nearly identical roughness (Fig. 8B, C), which is consistent with the similar distributions of contact numbers. Though previous studies showed that the (010) plane had the highest contact surface area [48, 49], the volume of collagen is much larger than these of polylactic acid and oleic acid, which hinders the binding of collagen onto (010) face with a half of the hydroxyl grouping shielded. Furthermore, the side chains of Pro and Gly are rigid and fail to penetrate into the groves in (010) face (Fig. 8D).

There are highly prominent hydroxyl groups at the (010), (110) and (1-10) surfaces, and the three hydroxyl groups on the pyranose ring are located at the equatorial position of the ring. Therefore, (010), (110) and (1-10) have significant hydrophilic properties and polarity. The (100) surface corresponds to the axial direction of the pyranose ring with hydrophobic C-H groups exposed to the surrounding medium and exhibits non-polarity. In the view of the large amount of hydroxyl groups and the polarity of Gly in collagen, electrostatic interactions may play an important role at the interface, particularly through hydrogen bonding. The number of hydrogen bonds between collagen and cellulose have been calculated. It has been found that even though there are a large number of hydroxyl groups in the surface of cellulose, few hydrogen bonds formed between cellulose and collagen are observed (Fig. 9). In terms of (010) face, one hydrogen bond occupancy is lower than 12% while two hydrogen bond occupancy is

lower than 0.5%. (110) and (1-10) faces display similar tendency to form hydrogen bonds with collagen and form less than 8% and 6% one hydrogen bond occupancy, respectively. (100) face display the least hydrogen bond among all the faces with occupancy less than 3%. Hydrogen bonding interactions between cellulose and collagen are limited due to steric hindrance. The sidechains of proline contact with the surface of cellulose, which hinders the interactions between backbone of collagen and cellulose. The results of hydrogen bonds interactions are different from the previous researches, which suggest that there are lots of hydrogen bonds so that they enhance the composite of cellulose and collagen [50, 51]. The difference in hydrogen bonding interactions may attribute to the distinctive primary structures of collagen and the abundance of hydroxyproline provide more sites to form hydrogen bonds.

It was interesting to note that the polar (110) and (1-10) faces formed hydrogen bonding linker with collagen participated by water molecules. As shown in Fig. 10C, water molecules between collagen and cellulose form hydrogen bonds with backbone carbonyl oxygen and hydroxyl group at the same time, connecting (110) face and collagen. The similar phenomenon has also been observed in the interface between (1-10) face and collagen with 3 water molecules involved in the network of hydrogen bonds. However, there is no hydrogen bonding linker observed in (100) and collagen. As shown in Fig. 10A, due to its hydrophobicity, few water molecules accumulate between collagen and (100) face, which prohibit the indirect connection through hydrogen bonding. It is intriguing to find that there is no hydrogen bond network connecting collagen and (010) face though the (010) face is hydrophilic. As shown in Fig. 10B, water molecules accumulate in the interface between (010) and collagen and most of water molecules are stuck in the deep groves. The steric confinement caused by the limited volumes of the groves restricts the freedom of water molecules and prohibits the formation of hydrogen bonds which require suitable distance and orientation.

In general, the polar (110) and (1-10) surfaces had the strongest affinity with collagen. Although there was a minimum number of hydroxyl groups on the (100) surface, the interaction of the surface C-H moiety with collagen can achieve a larger van der Waals interactions with the smoothest surface. The (010) face exhibits the weakest interactions with collagen. The affinity can be attributed to the cellulose surface structure and the corresponding contribution of indirect hydrogen bonding interactions. Direct hydrogen bonding interaction is not significantly contributive to the affinity. Selecting proper collagen with more hydroxyproline may promote hydrogen bonding interactions. Furthermore, surface modification to increase the polarity of cellulose may also be feasible to enhance the interactions between cellulose and collagen, which has been validated by previous study [52]. Adding crosslinking agent playing similar roles to water molecules is also a possible strategy to improve the property of cellulose/collagen composite.

4. Conclusion

The interfacial structure between cellulose and collagen is one of the key factors regulating the performance of composites. In order to better understand the composite material at the molecular level and control the performance of the composite material rationally, MD simulations were carried out to

investigate the interactions between cellulose and collagen. It has been observed that collagen was adsorbed onto the surface of cellulose without structural damage. (110) and (1-10) crystal faces exhibited the strongest affinity with collagen compared to the other two faces, which was attributed to combined effects of smooth surface and hydrogen bonding network involved water molecules. Van der Waals interactions and crosslinking effects of hydrogen bonding network codetermined the affinity between cellulose and collagen. Direct hydrogen bonding interactions were not the predominant force driving the binding with low occupancy. This study can provide insights into the interface properties of cellulose and collagen at the molecular level, which may shed light on the rational design of cellulose/collagen composite and promote the applications of the biomaterial.

Declarations

Authorship contribution statement

Lulu Ning and Zhijian Li conceived the idea, designed the experiments, evaluated data. Lulu Ning and Huaiqin Ma wrote the manuscript. Huaiqin Ma and Lulu Ning performed molecular dynamics simulations and carried out the analysis. All authors reviewed, approved and contributed to the manuscript finalization.

Funding

This work was financially supported by the Natural Science Basic Research Plan in Shaanxi Province of China (2021JQ-537).

Conflicts of interest

The authors declare no competing interests

References

1. French AD (2017) Glucose, not cellobiose, is the repeating unit of cellulose and why that is important. Cellulose 24: 4605-4609. https://doi:10.1007/s10570-017-1450-3
2. Ansari F, Sjöstedt A, Larsson PT, Berglund LA, Wågberg L (2015) Hierarchical wood cellulose fiber/epoxy biocomposites – Materials design of fiber porosity and nanostructure. Composites Part A: Applied Science and Manufacturing 74: 60-68. https://doi:10.1016/j.compositesa.2015.03.024
3. Moon RJ, Martini A, Nairn J, Simonsen J, Youngblood J (2011) Cellulose nanomaterials review: structure, properties and nanocomposites. Chemical Society reviews 40: 3941-3994. https://doi:10.1039/c0cs00108b
4. Toosi S, Naderi-Meshkin H, Kalalinia F, HosseinKhani H, Heirani-Tabasi A, Havakhah S, Nekooei S, Jafarian AH, Rezaie F, Peivandi MT, Mesgarani H, Behravan J (2019) Bone defect healing is induced by collagen sponge/polyglycolic acid. Journal of Materials Science: Materials in Medicine 30: 33. https://doi:10.1007/s10856-019-6235-9

5. Zhang W, Wang XC, Li XY, Zhang LL, Jiang F (2020) A 3D porous microsphere with multistage structure and component based on bacterial cellulose and collagen for bone tissue engineering. Carbohydr Polym 236: 116043. https://doi:10.1016/j.carbpol.2020.116043
6. Salimi S, Sotudeh-Gharebagh R, Zarghami R, Chan SY, Yuen KH (2019) Production of nanocellulose and its applications in drug delivery: A critical review. ACS Sustainable Chemistry & Engineering 7: 15800-15827. https://doi:10.1021/acssuschemeng.9b02744
7. Chen W, Yu H, Lee SY, Wei T, Li J, Fan Z (2018) Nanocellulose: a promising nanomaterial for advanced electrochemical energy storage. Chemical Society Reviews 47: 2837-2872. https://doi:10.1039/C7CS00790F
8. Zhao D, Zhu Y, Cheng W, Chen W, Wu Y, Yu H (2021) Cellulose-based flexible functional materials for emerging intelligent electronics. Advanced Materials 33: e2000619. https://doi:10.1002/adma.202000619
9. Golmohammadi H, Morales-Narváez E, Naghdi T, Merkoçi A (2017) Nanocellulose in sensing and biosensing. Chemistry of Materials 29: 5426-5446. https://doi:10.1021/acs.chemmater.7b01170
10. Sorushanova A, Delgado LM, Wu Z, Shologu N, Kshirsagar A, Raghunath R, Mullen AM, Bayon Y, Pandit A, Raghunath M, Zeugolis DI (2019) The Collagen Suprafamily: From Biosynthesis to Advanced Biomaterial Development. Advanced Materials 31: e1801651. https://doi:10.1002/adma.201801651
11. Henriksen K, Karsdal MA (2016) Type I collagen. Biochemistry of Collagen 1-11. https://doi:10.1016/b978-0-12-809847-9.00001-5
12. Lee A, Hudson AR, Shiwarski DJ, Tashman JW, Feinberg AW (2019) 3D bioprinting of collagen to rebuild components of the human heart. Science 365: 482-487.
13. Ge L, Xu Y, Li X, Yuan L, Tan H, Li D, Mu C (2018) Fabrication of antibacterial collagen-based composite wound dressing. ACS Sustainable Chemistry & Engineering 6: 9153-9166. https://doi:10.1021/acssuschemeng.8b01482
14. Pei Y, Yang J, Liu P, Xu M, Zhang X, Zhang L (2013) Fabrication, properties and bioapplications of cellulose/collagen hydrolysate composite films. Carbohydr Polym 92: 1752-1760. https://doi:10.1016/j.carbpol.2012.11.029
15. Noh YK, Dos Santos Da Costa A, Park YS, Du P, Kim IH, Park K (2019) Fabrication of bacterial cellulose-collagen composite scaffolds and their osteogenic effect on human mesenchymal stem cells. Carbohydr Polym 219: 210-218. https://doi:10.1016/j.carbpol.2019.05.039
16. Lee JS, Ryu YS, Kim IS, Kim SH (2019) Effect of interface affinity on the performance of a composite of microcrystalline cellulose and polypropylene/polylactide blends. Polymer International 68: 1402-1410. https://doi:10.1002/pi.5831
17. Nakatani H, Iwakura K, Hamadate M, Okazaki N, Aoyama M, Terano M (2011) Interface adhesion properties of syndiotactic polypropylene/cellulose group composite: Relationship between chemical structure of coupling agent and reactivity for cellulose group. Journal of Applied Polymer Science 122: 2798-2806. https://doi:10.1002/app.34325

18. Abitbol T, Rivkin A, Cao Y, Nevo Y, Abraham E, Ben-Shalom T, Lapidot S, Shoseyov O (2016) Nanocellulose, a tiny fiber with huge applications. Current Opinion in Biotechnology 39: 76-88. https://doi:10.1016/j.copbio.2016.01.002
19. Reinikainen T, Ruohonen L, Nevanen T, Laaksonen L, Kraulis P, Jones TA, Knowles JKC, Teeri TT (1992) Investigation of the function of mutated cellulose-binding domains of trichoderma reesei cellobiohydrolase I. Proteins 14: 475-482.
20. Markus L, Maija-Liisa M, Maarit K, Gunnar L, Jerry S, Torbjorn D, Tapani R, Goran P, Arto A (1995) Identification of functionally important amino acids in the cellulose-binding domain of Trichoderma reesei cellobiohydrolase I. Protein Science 4: 1056-1064.
21. Lehtio J, Sugiyamat J, Gustavsson M, Fransson L, Linder M, Teeri uT (2016) The binding specificity and affinity determinants of family 1 and family 3 cellulose b inding modules. Proceedings of the National Academy of Sciences of the United States of America 100: 484-489.
22. Griffo A, Rooijakkers BJM, Hahl H, Jacobs K, Linder MB, Laaksonen P (2019) Binding forces of cellulose binding modules on cellulosic nanomaterials. Biomacromolecules 20: 769-777. https://doi:10.1021/acs.biomac.8b01346
23. Chundawat SPS, Nemmaru B, Hackl M, Brady SK, Hilton MA, Johnson MM, Chang S, Lang MJ, Huh H, Lee SH, Yarbrough JM, Lopez CA, Gnanakaran S (2021) Molecular origins of reduced activity and binding commitment of processive cellulases and associated carbohydrate-binding proteins to cellulose III. Journal of Biological Chemistry 296: 100431. https://doi:10.1016/j.jbc.2021.100431
24. Zhang M, Ding C, Yang J, Lin S, Chen L, Huang L (2016) Study of interaction between water-soluble collagen and carboxymethyl cellulose in neutral aqueous solution. Carbohydr Polym 137: 410-417. https://doi:10.1016/j.carbpol.2015.10.098
25. Liu D, Dong X, Han B, Huang H, Qi M (2020) Cellulose nanocrystal/collagen hydrogels reinforced by anisotropic structure: Shear viscoelasticity and related strengthening mechanism. Composites Communications 21: 100374. https://doi:10.1016/j.coco.2020.100374
26. Fernandes A, Thomas L, Altaner C, Callow P, Forsyth V, Apperley D, Kennedy C, Jarvis M (2011) Nanostructure of Cellulose Microfibrils in Spruce Wood. Proceedings of the National Academy of Sciences 108: e1195-e1203. https://doi:10.1073/pnas
27. Vermaas JV, Crowley MF, Beckham GT (2019) A quantitative molecular atlas for interactions between lignin and cellulose. ACS Sustainable Chemistry & Engineering 7: 19570-19583. https://doi:10.1021/acssuschemeng.9b04648
28. Malaspina DC, Faraudo J (2019) Molecular insight into the wetting behavior and amphiphilic character of cellulose nanocrystals. Advances in Colloid and Interface Science 267: 15-25. https://doi:10.1016/j.cis.2019.02.003
29. Cevanti1. TA, Sari. NSP, Isnaini. SI, Rois. MF, Setyawan. H, Soetojo. A, Widjiastuti. I (2021) Cellulose fiber from coconut coir for development of dental composite filler. Journal of International Dental and Medical Research 14: 1401-1406.

30. Gomes TCF, Skaf MS (2012) Cellulose-builder: A toolkit for building crystalline structures of cellulose. Journal of Computational Chemistry 33: 1338-1346. https://doi:10.1002/jcc.22959
31. Berisio R, Vitagliano L, Mazzarella L, Zagari A (2009) Crystal structure of the collagen triple helix model $[(Pro\text{-}Pro\text{-}Gly)_{10}]_3$. Protein Science 11: 262-270. https://doi:10.1110/ps.32602
32. Humphrey W, Dalke A, Schulten K (1996) VMD: Visual molecular dynamics. Journal of Molecular Graphics & Modelling 14: 33-38.
33. Mark P, Nilsson L (2001) Structure and dynamics of the TIP3P, SPC, and SPC/E water models at 298 K. The Journal of Physical Chemistry A 105: 9954-9960.
34. Boonstra S, Onck PR, van der Giessen E (2016) CHARMM TIP3P water model suppresses peptide folding by solvating the unfolded state. The Journal of Physical Chemistry B 120: 3692-3698. https://doi:10.1021/acs.jpcb.6b01316
35. Lee S, Tran A, Allsopp M, Lim JB, Hénin J, Klauda JB (2014) CHARMM36 united atom chain model for lipids and surfactants. The Journal of Physical Chemistry B 118: 547-556. https://doi:10.1021/jp410344g
36. Van Der Spoel D, Lindahl E, Hess B, Groenhof G, Mark AE, Berendsen HJ (2005) GROMACS: Fast, flexible, and free. Journal of Computational Chemistry 26: 1701-1718. https://doi:10.1002/jcc.20291
37. Berendsen HJC, Spoel Dvd, Drunen Rv (1995) GROMACS: A message-passing parallel molecular dynamics implementation. Computer Physics Communications 91 43-56.
38. Petersen HG (1995) Accuracy and efficiency of the particle mesh Ewald method. The Journal of Chemical Physics 103: 3668-3679. https://doi:10.1063/1.470043
39. Hess B, Bekker H, Berendsen H, Fraaije J (1998) LINCS: A linear constraint solver for molecular simulations. Journal of Computational Chemistry 18: 1463–1472.
40. Berendsen HJC, Postma JPM, van Gunsteren WF, DiNola A, Haak JR (1984) Molecular dynamics with coupling to an external bath. The Journal of Chemical Physics 81: 3684-3690. https://doi:10.1063/1.448118
41. Nosé S, Klein ML (2006) Constant pressure molecular dynamics for molecular systems. Molecular Physics 50: 1055-1076. https://doi:10.1080/00268978300102851
42. Parrinello M, Rahman A (1981) Polymorphic transitions in single crystals: A new molecular dynamics method. Journal of Applied Physics 52: 7182-7190. https://doi:10.1063/1.328693
43. Roux B (1995) The calculation of the potential of mean force using computer simulations. Computer Physics Communications 91: 275-282. https://doi:10.1016/0010-4655(95)00053-I
44. Hub JS (2015) g_wham—A free weighted histogram analysis implementation including robust error and autocorrelation estimates. Journal of Chemical Physics 6: 3713-3720.
45. Cosgrove DJ (2014) Re-constructing our models of cellulose and primary cell wall assembly. Curr Opin Plant Biol 22: 122-131. https://doi:10.1016/j.pbi.2014.11.001
46. W.W.Hooft R, Sander C, Vrien G (1997) Objectively judging the quality of a protein structure from a Ramachandran plot. Computer Applications in the Biosciences Cabios 13: 425-430.

47. Köppen S, Ohler B, Langel W (2007) Adsorption of collagen fragments on titanium oxide surfaces: A molecular dynamics study. Zeitschrift für Physikalische Chemie 221: 3-20. https://doi:10.1524/zpch.2007.221.1.3
48. Quddus MA, Rojas OJ, Pasquinelli MA (2014) Molecular dynamics simulations of the adhesion of a thin annealed film of oleic acid onto crystalline cellulose. Biomacromolecules 15: 147614-147683. https://doi:10.1021/bm500088c
49. Ren Z, Guo R, Bi H, Jia X, Xu M, Cai L (2020) Interfacial adhesion of polylactic acid on cellulose surface: A molecular dynamics study. ACS Appl Mater Interfaces 12: 3236-3244. https://doi:10.1021/acsami.9b20101
50. Rudisill SG, DiVito MD, Hubel A, Stein A (2015) In vitro collagen fibril alignment via incorporation of nanocrystalline cellulose. Acta Biomater 12: 122-128. https://doi:10.1016/j.actbio.2014.10.024
51. Zhang M, Chen L, Ding C, Yang H, Huang L (2014) Interactions of collagen and cellulose in their blends with 1-ethyl-3-methylimidazolium acetate as solvent. Cellulose 21: 3311-3322. https://doi:10.1007/s10570-014-0372-6
52. Wang W, Zhang X, Li C, Du G, Zhang H, Ni Y (2018) Using carboxylated cellulose nanofibers to enhance mechanical and barrier properties of collagen fiber film by electrostatic interaction. J Sci Food Agric 98: 3089-3097. https://doi:10.1002/jsfa.8809

Figures

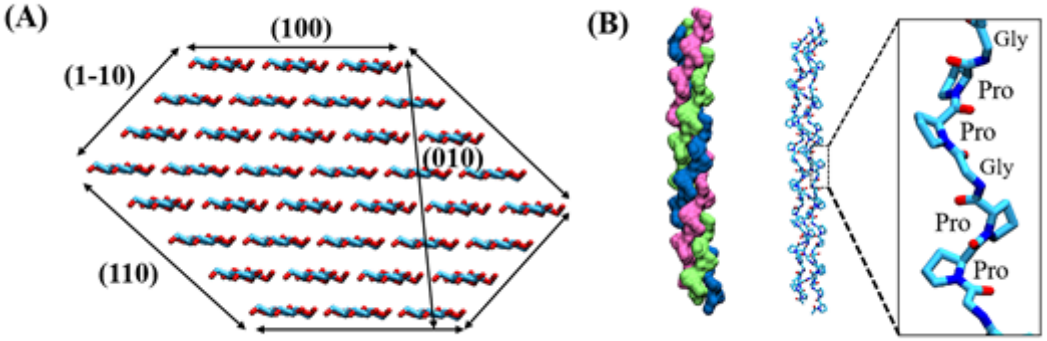

Figure 1

(**A**) Schematic presentation of the organization of cellulose Iβ with crystal faces labeled and hydrogen atoms were omitted for clarity. Oxygen atoms are red, and carbon atoms are cyan. (**B**) Initial structure of collagen with residue names labeled (PDB ID: 1K6F).

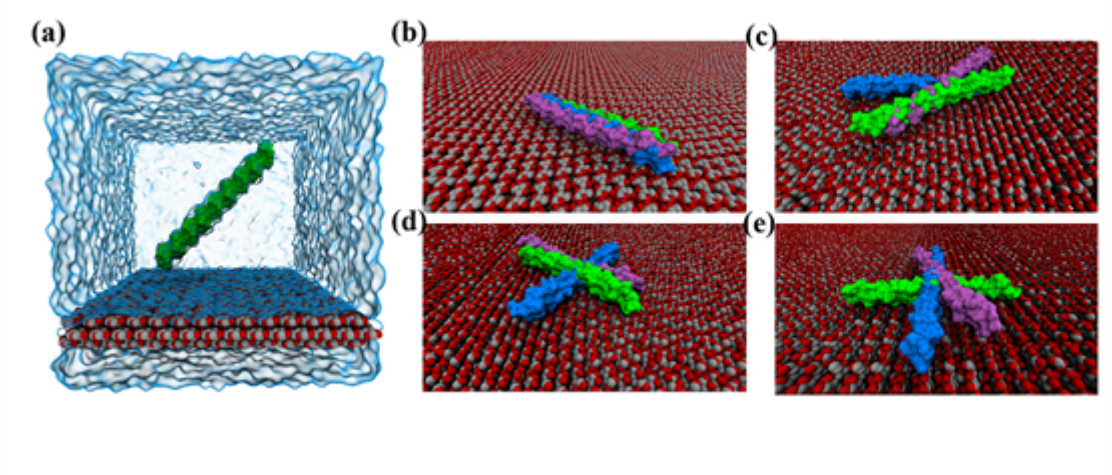

Figure 2

(**A**) Illustration for a single constructed system with collagen above (100) crystal face. The water molecules are represented as a blue surface. (**B**)-(**E**) Last snapshots of the collagens above (100), (110), (1-10) and (010) crystal faces. All collagens were drawn as surface in green (0°), purple (30°), and blue (45°) to represent the three replicas of MD simulations. The atoms of cellulose are shown as spheres with carbon in gray and oxygen in red, hydrogen is not shown for clarity.

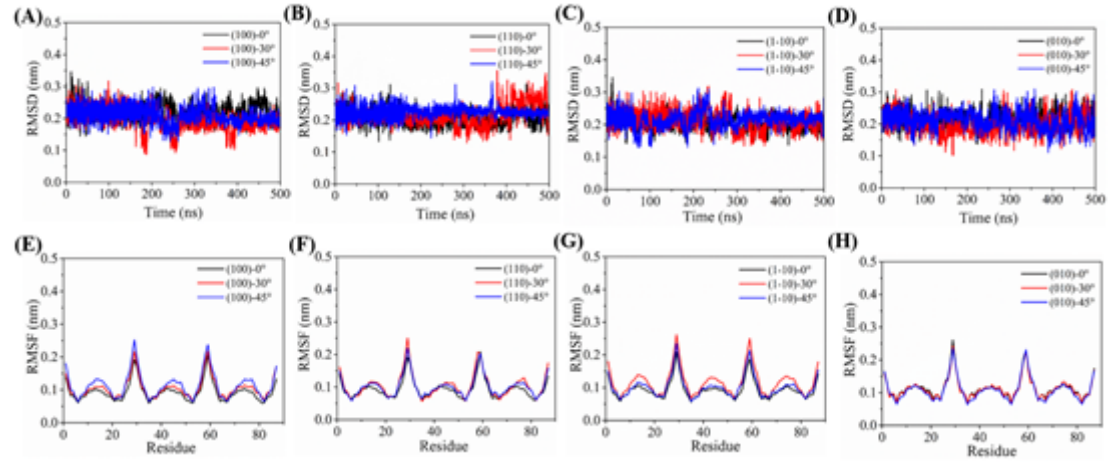

Figure 3

(**A**)-(**D**) Time evolution of RMSD values of collagen on (100), (110), (1-10) and (010) faces over time, respectively. (**E**)-(**H**) RMSF variation of each residue that constitutes collagen on different crystal faces.

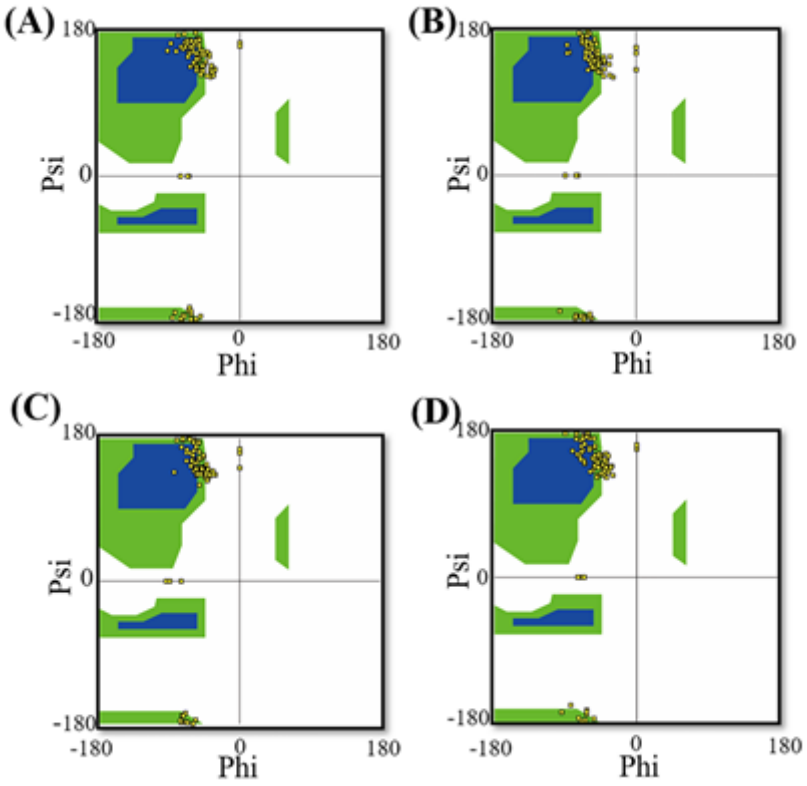

Figure 4

The Ramachandran plots of collagens adsorbed on (**A**)(100), (**B**) (110), (**C**) (1-10), and (**D**) (010) faces.

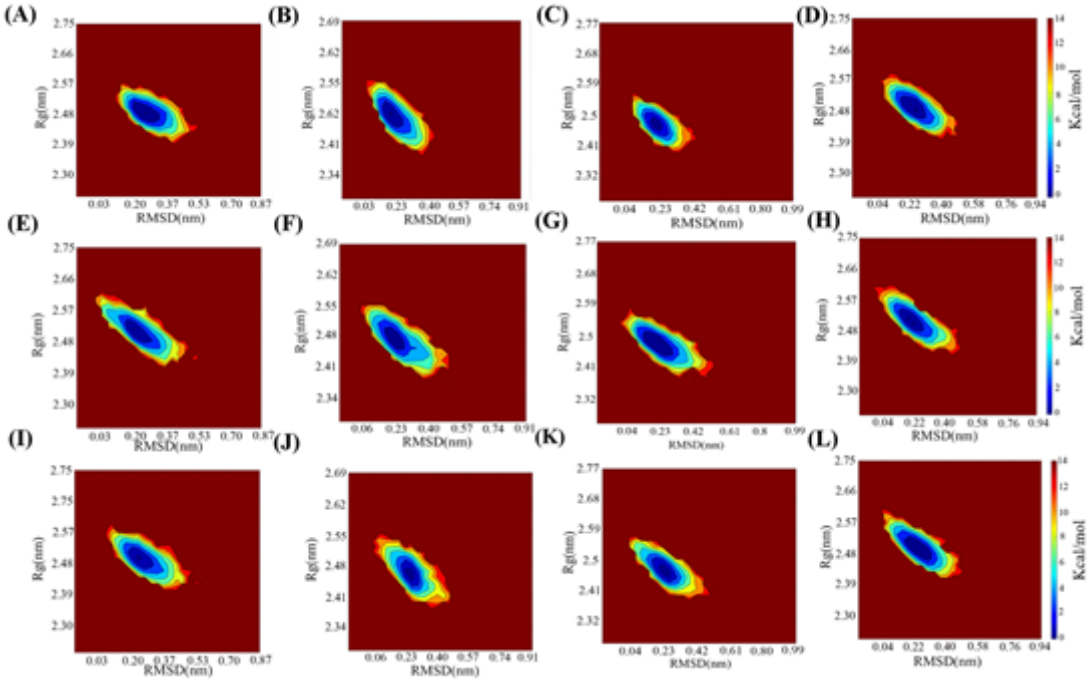

Figure 5

Free energy landscape of all model collagens with RMAD and Rg as reaction coordinates. The columns from left to right represent (100), (110), (1-10) and (010) faces, respectively. The rows from top to bottom represent collagens with 0°, 30°, and 45° from cellulose crystalline faces, respectively.

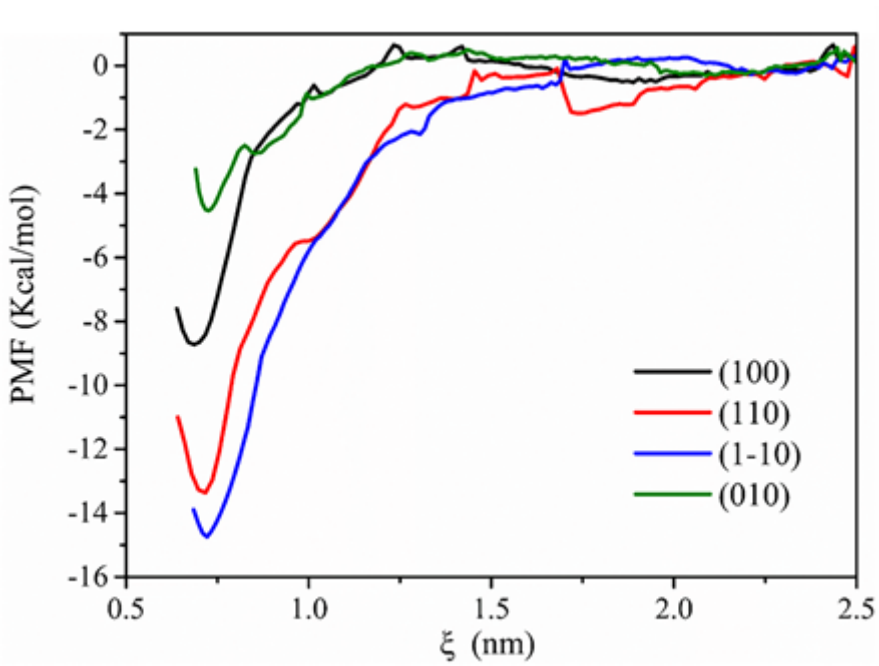

Figure 6

Potential of mean force plots describing the binding of collagen and cellulose.

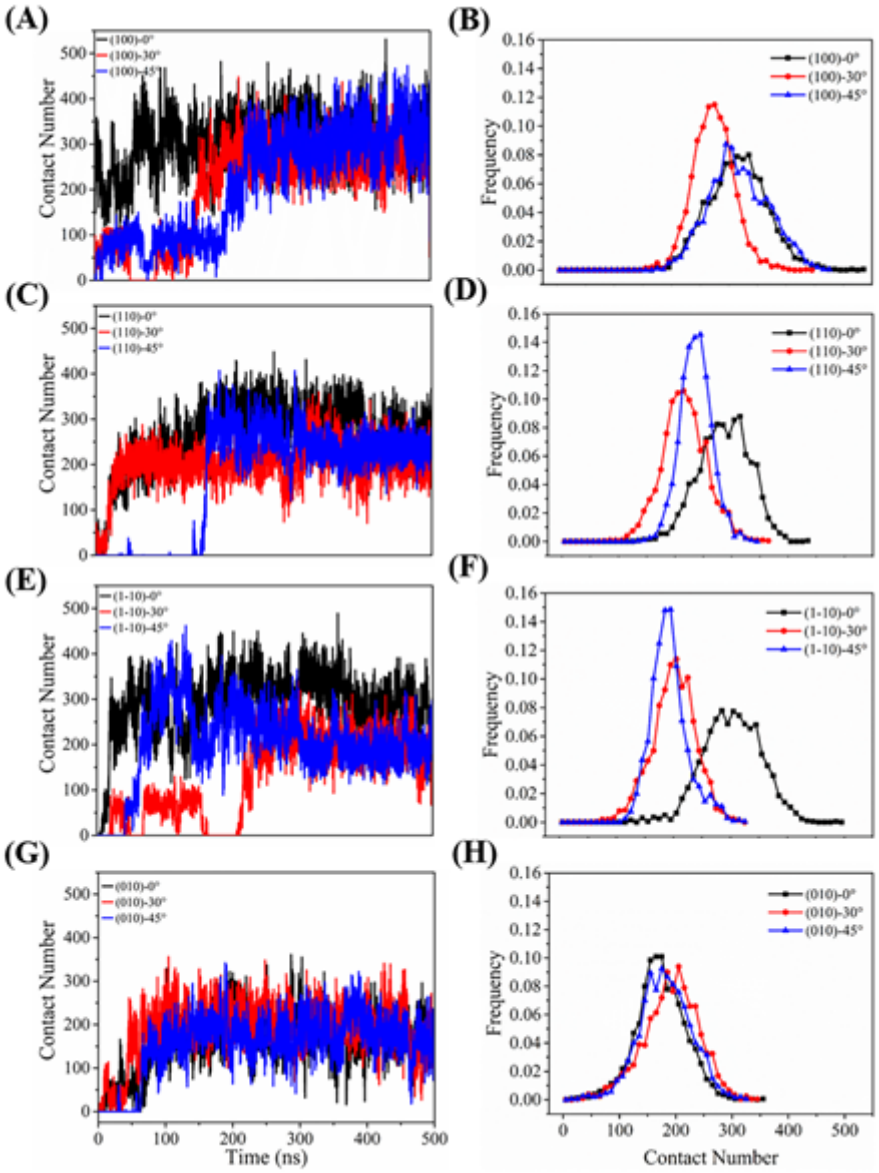

Figure 7

Changes of heavy atomic contact number of collagens on (100) (**A**), (110) (**C**), (1-10) (**E**), (010) (**G**)faces over time. (**B**), (**D**), (**F**), (**H**) are the distributions of heavy atomic contact number of collagens on the corresponding crystal planes.

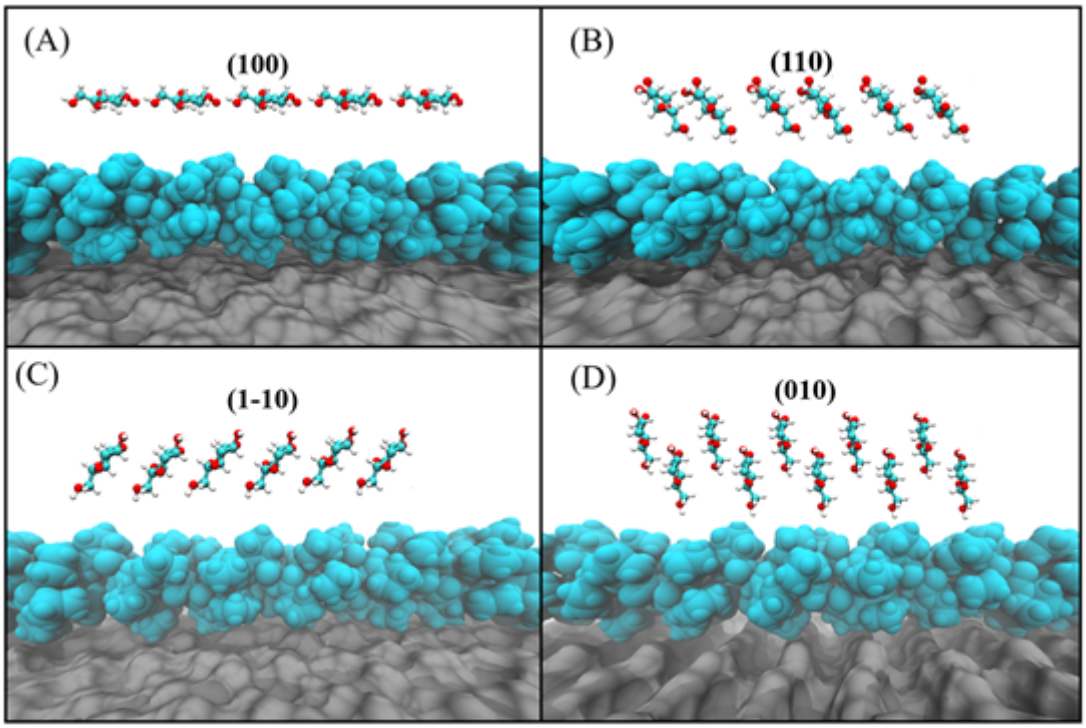

Figure 8

Surface topography of cellulose (100) (**A**), (110) (**B**), (1-10) (**C**), (010) (**D**) with crystal plane and protein illustrated. Blue represents collagen, gray represents cellulose.

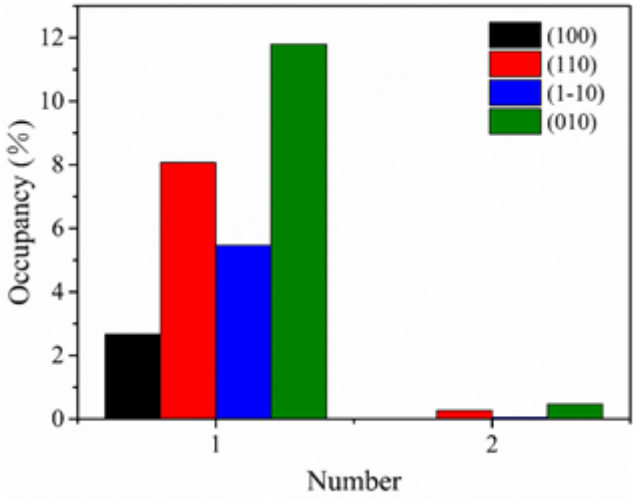

Figure 9

Hydrogen bond occupancy between collagen and cellulose crystalline faces.

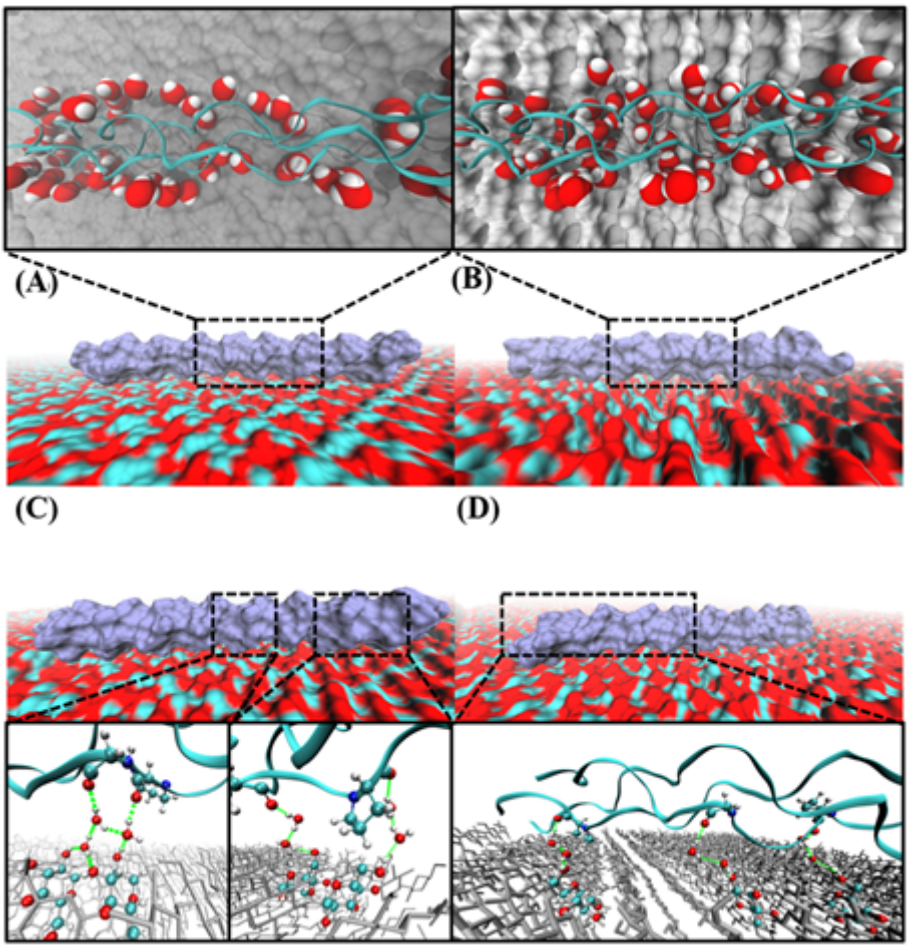

Figure 10

Hydrogen bond interaction formed by water molecules between collagen and different cellulose surfaces (**A**) (100), (**B**) (010), (**C**) (110), (**D**) (1-10).

Supplementary Files

This is a list of supplementary files associated with this preprint. Click to download.

- TOC.png